TITLE: Sampling the conformational landscapes of transporters and receptors with AlphaFold2

AUTHORS: Diego del Alamo* (1,2), Davide Sala* (3), Hassane S. Mchaourab† (1), Jens Meiler† (2,3)
1. Department of Molecular Physiology and Biophysics, Vanderbilt University, Nashville, TN, USA
2. Department of Chemistry, Vanderbilt University, Nashville, TN, USA
3. Institute for Drug Discovery, Leipzig University, Leipzig, DE

* Equal contribution
† Correspondence: hassane.mchaourab@vanderbilt.edu, jens@meilerlab.org

ABSTRACT

Equilibrium fluctuations and triggered conformational changes often underlie the functional cycles of membrane proteins. For example, transporters mediate the passage of molecules across cell membranes by alternating between inward-facing (IF) and outward-facing (OF) states, while receptors undergo intracellular structural rearrangements that initiate signaling cascades. Although the conformational plasticity of these proteins has historically posed a challenge for traditional *de novo* protein structure prediction pipelines, the recent success of AlphaFold2 (AF2) in CASP14 culminated in the modeling of a transporter in multiple conformations to high accuracy. Given that AF2 was designed to predict static structures of proteins, it remains unclear if this result represents an underexplored capability to accurately predict multiple conformations and/or structural heterogeneity. Here, we present an approach to drive AF2 to sample alternative conformations of topologically diverse transporters and G-protein coupled receptors (GPCRs) that are absent from the AF2 training set. Whereas models generated using the default AF2 pipeline are conformationally homogeneous and nearly identical to one another, reducing the depth of the input multiple sequence alignments (MSAs) by stochastic subsampling led to the generation of accurate models in multiple conformations. In our benchmark, these conformations spanned the range between two experimental structures of interest, with models at the extremes of these conformational distributions observed to be among the most accurate (average template modeling (TM)-score of 0.94). These results suggest a straightforward approach to identifying native-like alternative states, while also highlighting the need for the next generation of deep learning algorithms to be designed to predict ensembles of biophysically relevant states.

INTRODUCTION

Dynamic interconversion between multiple conformations underpins the functions of integral membrane proteins in all domains of life[1–4]. For example, the vectorial translocation of substrates by transporters is mediated by movements that open and close extracellular and intracellular gates[5,6]. For GPCRs, ligand binding on the extracellular side triggers structural rearrangements on the intracellular side that initiate downstream signaling[7,8]. Traditional computational prediction pipelines reliant on inter-residue distance restraints calculated from deep MSAs have historically struggled to accurately predict the structures of these proteins and their

movements. The resulting models are unnaturally compact and frequently distorted, preventing critical questions about ligand and/or drug binding modes from being addressed[9,10].

A performance breakthrough was unveiled during CASP14 by AF2[11–13], which achieved remarkably accurate *de novo* structure prediction. Upon examining the list of CASP14 targets and corresponding models, we found that AF2 modeled the multidrug transporter LmrP (target T1024) in multiple conformations, two of which were individually consistent with published experimental data[14–18]. This observation stimulated the question of whether such performance can be duplicated for other membrane proteins. At its essence, this question centers on whether AF2 can sample the conformational landscape in the minimum energy basin. Here, we investigate this hypothesis using a benchmark set of topologically diverse transporters and GPCRs. Our results demonstrate that reducing the depth of the input MSAs is conducive to the generation of accurate models in multiple conformations by AF2, suggesting that the algorithm's outstanding predictive performance can be extended to sample alternative structures of the same target. For most proteins considered, we report a striking correlation between the breadth of structures predicted by AF2 and the corresponding cryo-EM and/or X-ray crystal structures. Finally, we propose a modeling pipeline for researchers interested in sampling alternative conformations of specific membrane proteins, which we apply to the structurally unknown GPR114/AGRG5 adhesion GPCR as an example.

RESULTS AND DISCUSSION

The default three-stage AF2 pipeline consists of 1) querying of sequence databases and generation of an MSA, 2) inference via a neural network using a randomly resampled subset of this MSA containing up to 5120 sequences, which is repeated three times (a process termed "recycling"), and 3) resolution of steric clashes and bond geometry using a constrained all-atom molecular dynamics simulation. The neural networks used for prediction were trained on all structures deposited in the Protein Data Bank (PDB) on or before April 30th, 2018[11]. Therefore, by necessity, this study is restricted to proteins whose structures were absent from the PDB before this date and have since been determined at atomic resolution in two or more conformations. We selected five transporters that not only met these criteria but also reflected a range of transport mechanisms characterized in the literature[5], including rocking-bundle (LAT1[19,20], ZnT8[21]), rocker-switch (MCT1[22], STP10[23]), and elevator (ASCT2[24,25]). We also included three GPCRs, which were distributed across classes A (CGRPR[26,27]), B1 (PTH1R[28,29]), and F (FZD7[30]; to serve as points of comparison, we used the active conformation of FZD7 and the inactive conformation of the nearly identical FZD4[31]).

AF2 generates multiple conformations of all eight target proteins

The sequences of all targets were truncated at the N- and C-termini to remove large soluble and/or intrinsically disordered regions which represent a challenge for AF2 (see *Methods*). The structures were then predicted using the default AF2 structure prediction pipeline in the absence of templates. However, the resulting models were largely identical to one another and failed to shed light on the target protein's conformational space. To diversify the models generated by AF2, we reduced the number of recycles to one and restricted the depth of the randomly subsampled MSAs to contain as few as 16 sequences. To sample the conformational landscape more exhaustively, we generated fifty models of each protein for each MSA size, while skipping the final MD simulation to reduce the pipeline's total computational cost. For the targets, each model's similarity to the experimental structures was quantified using template modeling (TM)-score[32–34], a metric ranging

from 0 to 1, which indicates how well the two backbone (C_α atoms) structures superimpose over one another (higher values corresponding to greater similarity; Figure 1A).

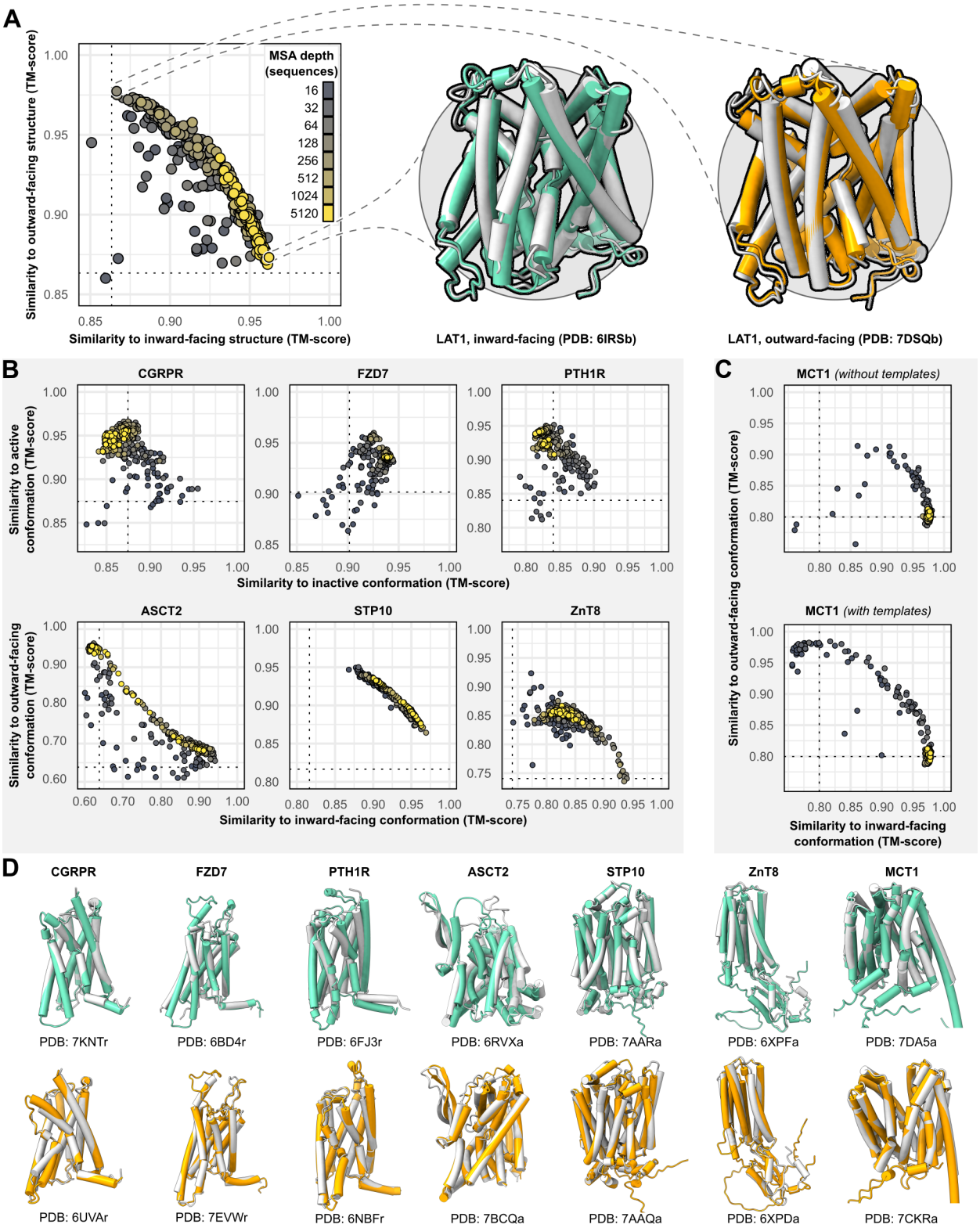

Figure 1. Alternative conformations of transporters and GPCRs can be predicted by AF2. (A) Representative models of the transporter LAT1 in IF and OF conformations. Experimental structures shown in gray and models shown in colors. **(B)** Comparison of AF2 models with inactive/active or IF/OF experimental structures as a function of MSA depth for GPCRs (top) and transporters (bottom), respectively. All models shown here were generated without templates. Dashed lines indicate the TM-score between experimental structures and are shown for reference. (C) Supplementing shallow MSAs with OF templates allows AF2 to predict the OF conformation of MCT1. (D) Experimental structures superimposed over models with the greatest TM-scores. Inactive/IF and active/OF cartoons shown on the top and bottom in teal and orange, respectively.

Accurate models of all eight protein targets were obtained for at least one conformation (TM-score ≥0.9), consistent with published performance statistics (Figure 1B). MSAs with hundreds or thousands of sequences were generally observed to engender tighter clustering in conformations specific to each protein. Decreasing the depth of the subsampled MSAs, by contrast, appeared to promote the generation of alternative conformations. The increased diversity coincided with the generation of misfolded or outlier models. However, unlike the models of interest that resembled experimentally determined structures, misfolded models virtually never co-clustered and could thus be identified and excluded from further analysis (example shown in Figure 1 - figure supplement 1). Increasing the depth of subsampled MSAs had the desirable effect of eliminating these models, while also limiting the extent to which alternative conformations were sampled. Thus, our results revealed a delicate balance that must be achieved to generate models that are both diverse and natively folded. No general pattern was readily apparent regarding the ideal MSA depth required to achieve this balance, even when accounting for sequence length of the target (Figure 1 - figure supplement 2).

One target, MCT1, was exclusively modeled by AF2 in either IF or fully occluded conformations; over 99% of the models had TM-scores of ≥0.9 and <0.9 to the IF and OF structures, respectively, regardless of MSA depth. Therefore, we investigated the effect of providing templates of homologs in exclusively OF conformations alongside MSAs of various sizes (see *Methods* for details on template selection). Accurate OF models were obtained only with MSAs containing 16 to 32 sequences and constituted a minor population in an ensemble dominated by IF models. Thus, the generation of large numbers of models appeared to be necessary to yield intermediate conformations of interest. Similar results were observed when we modeled PTH1R using either inactive or active templates, as well as LAT1 using either OF or IF templates (Figure 1 - figure supplement 3), further indicating that the information content provided by the templates diminishes as the depth of the MSA increases.

Overall, these results demonstrate that both conformations of all eight protein targets could be predicted with AF2 to high accuracy (TM-score ≥0.9) by using MSAs that are far shallower than the default. However, because the optimal MSA depth and choice of templates varied for each protein, these parameters need to be explored for conformational sampling of a particular target.

<u>Predicted conformational fluctuations correlate with implied conformational dynamics</u>

To further investigate the structural heterogeneity predicted by these models, we calculated each residue's root mean squared deviation (RMSD) between the two experimental structures, as well as their root mean squared fluctuation (RMSF) among all fifty models following structure-based alignment (Figure 2). Correlation between these two measures were observed in most cases

and was notable for ASCT2, LAT1, CGRPR, and MCT1 with templates ($R^2 \geq 0.75$). The exception was MCT1 without templates, which was likely due to a lack of conformational diversity among the sampled models. The inclusion of templates restored this correlation in MCT1 but contributed negligibly to those of PTH1R and LAT1 (Figure 2 - figure supplement 1). The correlation demonstrates that predicted flexibility by AF2 is related to the protein's dynamics inferred from the experimental structures. In contrast with a recent preprint[35], the predicted flexibility values failed to correlate with their pLDDT values, which reflect the confidence of the AF2 prediction of each residue's local environment[36].

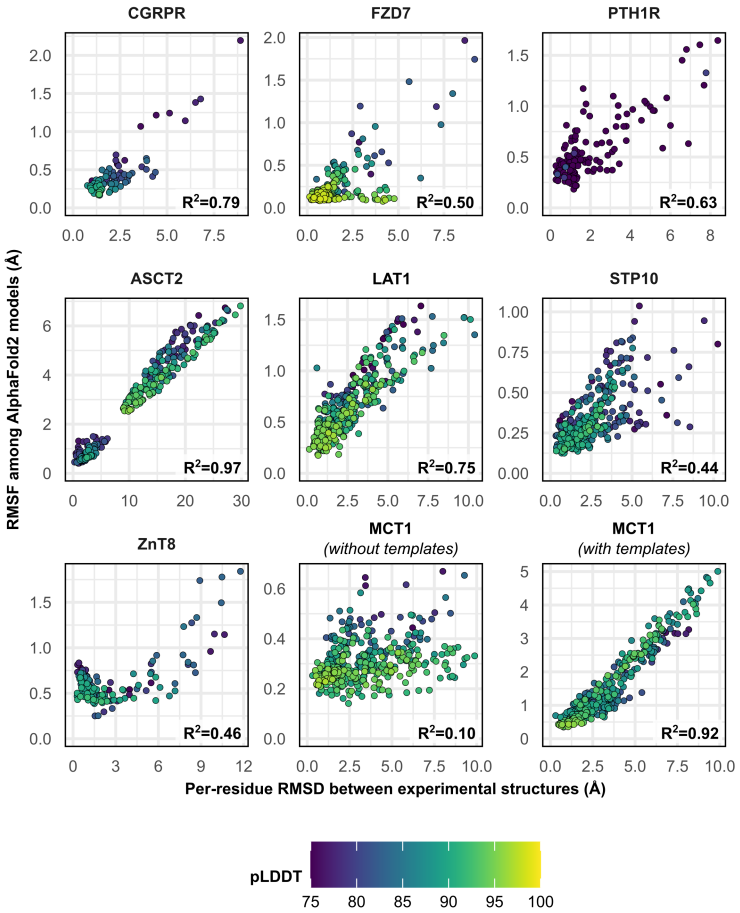

Figure 2. Comparison between each residue's C_α-RMSD in the two experimental structures and their RMSF values among AF2 models. Residues with low confidence (pLDDT $\leq$75) were omitted from this plot for all proteins except PTH1R. MSA sizes of 128 sequences were used for all predictions, except for MCT1 with templates, which instead used 32 sequences to capture the OF conformation. pLDDT refers to each residue's predicted accuracy, with a value of 100 indicating maximum confidence.

<u>Distributions of predicted models relative to the experimental structures</u>

Visual examination suggested that many of the predicted models fall "in between" the two experimentally determined conformations (example shown in Figure 3A). Furthermore, certain structural features expected to be conformationally heterogeneous, such as long loops, appeared to

be nearly identical across these models. Both observations raised questions about the relationship between the diversity of the predicted models and the breadth of the conformational ensembles bracketed by the experimental structures. To quantitatively place the predicted conformational variance in the context of the experimentally determined structures, we used principal component analysis (PCA), which reduces the multidimensional space to a smaller space representative of the main conformational motions. In our benchmark set, the first principal component (PC1) captured 64.9±16.1% of the structural variations among the models generated using MSAs with 32 or more sequences (Figure 3B), while comparison of PC1/PC2 values suggested that the predicted dynamics deviate from simple interpolation of two end states (Figure 3 - figure supplement 1). The experimental structures virtually always occupied well defined extreme positions. In every case, a correlation was evident between each model's PC1 values and their TM-scores. Indeed, the models with the most extreme PC1 values were also among the most accurate: average TM-scores were 0.94 for the top one, top three and top ten PC1 models, and Pearson correlation coefficients between PC1 and TM-scores of the ensemble of models exceeded 0.8 for all transporters in this dataset. Moreover, the experimental structures virtually always flanked the AF2 models along PC1. The exception, PTH1R, was determined in a partially inactive and active conformation[29], suggesting that models extending beyond the former state along PC1 may represent the fully inactive conformation. Therefore, these results indicate that accurate representative models of conformations of interest can be selected from the extreme positions along PC1.

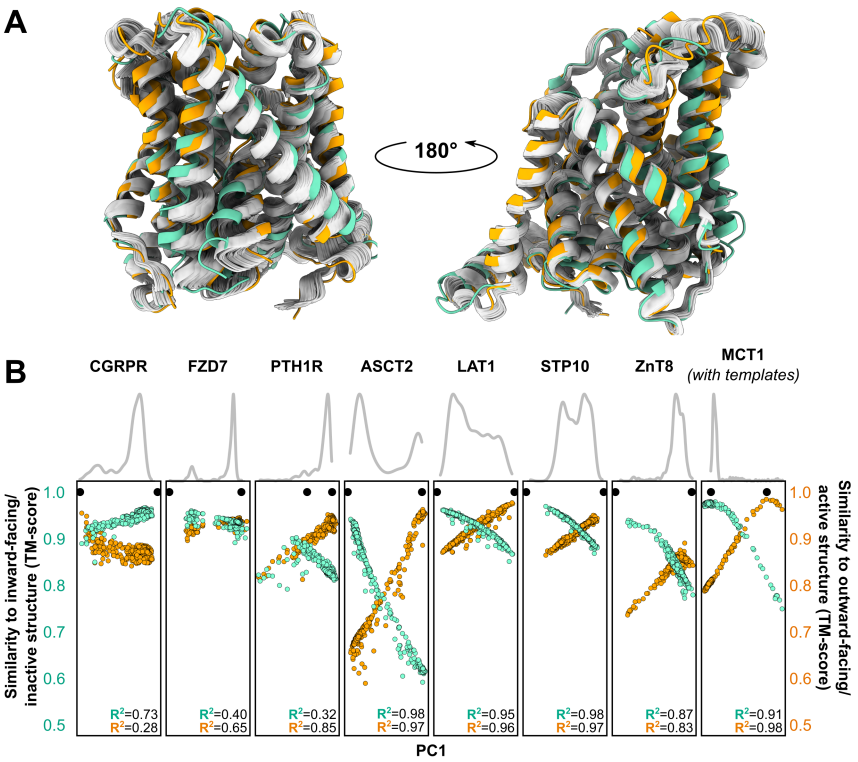

Figure 3. Distinct conformations can be delineated using PCA. (A) Conformational heterogeneity in AF2 models of LAT1. Experimental IF and OF conformations shown in teal and orange, respectively, while the gallery of AF2 models generated using 128 sequences are shown in gray. **(B)** Distribution of AF2 models generated using MSAs with 32 or more sequences across the first principal component (PC1) following PCA (gray traces). Scatter plots comparing each

model's position along PC1 and its structural similarity to experimentally determined structures. Teal: Similarity to IF (transporters) or inactive (GPCRs) conformation. Orange: Similarity to OF (transporters) or active (GPCRs) conformation. Each model is shown twice, once in teal and once in orange. Native structures are shown as black dots.

Limited conformational sampling is observed for proteins with structures in the AF2 training set

A follow-up question centers on whether this strategy can yield similar results for proteins with one conformation present in the AF2 training set. We investigated this question using four membrane proteins with two experimentally determined conformations, at least one of which was included in the AF2 training set: the class A GPCR CCR5[37,38], the serotonin transporter SERT[39,40], the multidrug transporter PfMATE[41,42], and the lipid flippase MurJ[43,44]. Using the template-free prediction pipeline outlined above, we determined the resultant models' similarity to the structures included in and absent from the training set. Unlike the results presented above, the majority of the transporter models generated this way were more similar to the conformation present in the training set than the conformation absent from the training set (i.e., their TM-scores were greater; Figure 1 - figure supplement 4). The conformational diversity of these models, including those generated using shallow MSAs, was far more limited than what was generally observed for the proteins discussed above, with the exception of MCT1 (Figure 1 - figure supplement 2). Although conformational diversity was demonstrated to a limited extent by the generation of occluded models of MurJ and PfMATE, none of the models observed adopted the alternative conformer. By contrast, while models of CCR5 were less biased toward the training set conformation, deep MSAs reduced conformational diversity. This divergence in performance may stem from the composition of the AF2 training set, which featured the structures of many active GPCRs but no structures, for example, of inward-facing MATEs[45].

Concluding remarks: proposed workflow and future directions

Our results indicate that the state-of-the-art *de novo* structural modeling algorithm AF2 can be manipulated to accurately model alternative conformations of transporters and GPCRs whose structures were not available in the training set. The use of shallow MSAs was instrumental to obtaining structurally diverse models, and in one case (MCT1) accurate modeling of alternative conformations also required the manual curation of template models. Thus, while the results presented here provide a blueprint for obtaining AF2 models of alternative conformations, they also argue against an optimal one-size-fits-all approach for sampling the conformational space of every protein with high accuracy. Indeed, whereas the DeepMind team reportedly required templates to obtain models of LmrP in an OF conformation[14], we found that this procedure was usually unnecessary. Accurate representatives of distinct conformers were generally obtainable with exhaustive sampling and could be identified by performing PCA and selecting models at the extreme positions of PC1. Nevertheless, prediction pipelines will likely require a combination of iterative fine-tuning specific to each target of interest followed by experimental verification to identify proposed conformers. Moreover, this approach showed limited success when applied to transporters whose structures were used to train AF2, hinting at the possibility that traditional methods may still be required to capture alternative conformers[46,47].

As a final verification of this proposed pipeline, we tested it on GPR114/AGRG5, a class B2 adhesion GPCR whose structure has not been experimentally determined. The structural model deposited in the AF2 database, which likely depicts an active conformation that diverges from the

structure of the homolog GPR97[48], could be recapitulated by using deep MSAs. The use of shallow MSAs (≤64 sequences), by contrast, yielded a range of intermediate conformations distributed across three well-separated clusters (Figure 3 - figure supplement 2). One of these clusters contains models with an orientation of TM6 and TM7 that fully occludes the orthosteric site and partially blocks the cytosolic pocket where G-proteins bind. The physiological relevance of these proposed structural movements nonetheless requires experimental validation.

While these results reinforce the notion that AF2 can provide models to guide biophysical studies of conformationally heterogeneous membrane proteins, they represent a methodological "hack", rather than an explicit objective built into the algorithm's architecture. Several preprints have provided evidence that AF2, despite its accuracy, likely does not learn the energy landscapes underpinning protein folding and function[35,49,50]. Moreover, AF2 does not directly account for the lipid environment, which have been experimentally shown to bias the conformational equilibria of membrane proteins[51–53]. As our results show that exploration of the conformational space is in part a byproduct of low sequence information provided for inference, they highlight the need for further development of artificial intelligence methods capable of learning the conformational flexibility intrinsic to protein structures.

METHODS

Overview of the prediction pipeline

Prediction runs were executed using AlphaFold v2.0.1 and a modified version of ColabFold[54] that is available at www.github.com/delalamo/af2_conformations. The pipeline used in this study differs from the default AF2 pipeline in several aspects. First, all MSAs were obtained using the MMSeqs2 server[55], rather than the default databases. Second, template search was disabled, except when explicitly performed with specific templates of interest (see below). Third, the number of recycles was set to one, rather than three by default. Finally, models were not refined following their prediction. Unlike the ColabFold pipeline, however, this study utilized all five neural networks when predicting structures without templates, with ten predictions per neural network per MSA size. Additionally, as only two of the five neural networks can use templates to supplement MSAs for structure prediction, they each performed twenty-five predictions per MSA size when performing template-based predictions. The following residues were omitted from modeling: 1-131 and 401-461 of CGRPR, 1-247 of FZD7, 1-175 and 492-593 of PTH1R, and 1-49 of LAT1.

MSA subsampling

MSA subsampling was carried out randomly by AF2, and depth values were controlled by modifying "*max_msa_clusters*" and "*max_extra_msa*" parameters prior to execution. The former parameter determines the number of randomly chosen sequence clusters provided to the AF2 neural network. The latter parameter determines the number of extra sequences used to compute additional summary statistics. Throughout this manuscript, we refer to the latter when describing the depth of the MSA used for prediction and set the former to half this value in all cases except when 5120 sequences were used, in which case we set the former to 512. No manual intervention was carried out to fine-tune the composition of these alignments.

Template-based predictions

Templates were fetched using the MMSeqs2 server used by ColabFold. All templates were manually inspected, and those with structures similar to the desired conformation of interest were retained. The following templates were used: outward-facing MCT1 with FucB (PDB 3O7Pa and 3O7Qa, 18% sequence identity calculated using Needleman Wunsch[56,57]); outward-facing LAT1 with AdiC (3OB6a and 5J4Ib, 22%); inward-facing LAT1 with b(0,+)AT1 (6LI9, 45%), KCC3 (6Y5Ra, 12%), GkApcT (6F34a, 24%), NKCC1 (6NPLa, 6PZTa, and 6NPHa, 12%), BasC (6F2Ga and 6F2Wa, 29%), and GadC (4DJIa and 4DJKb, 21%); active PTH1R with GCGR (6LMLr and 6VCBr, 30%) PAC1 (6M1I, 34%), and CRF1 (6P9X, 34%); inactive PTH1R with GLP1 (6LN2, 30%) and GCGR (5YQZ, 5XF1, and 5EE7, 28%). Template processing then proceeded as previously described, except that the parameter "*subsample_templates*" was set to True and the template similarity cutoff was reduced from 10% to 1%. Additionally, as only two of the five AF2 neural networks were parametrized to use templates, each of these two neural networks generated twenty-five models in order to arrive at fifty total models per MSA depth.

Structural analysis

TM-scores were calculated using TM-align[33]. Principal component analysis and RMSF calculations were carried out in CPPTRAJ[58]. Loop residues were omitted from PCA.

ACKNOWLEDGEMENTS

This study was funded by the National Institutes of Health (HSM: GM 128087) and the Deutsche Forschungsgemeinschaft (DFG, German Research Foundation) through CRC 1423, project number 421152132, subproject Z04. The authors would like to thank Dr. John Jumper for explaining how the DeepMind team predicted the structure of LmrP in CASP14 and Mr. Taylor Jones for helpful discussions on modeling MCT1 without templates.

BIBLIOGRAPHY

1. Campbell, E. *et al.* The role of protein dynamics in the evolution of new enzyme function. *Nat. Chem. Biol.* **12**, 944–950 (2016).
2. Cournia, Z. *et al.* Membrane Protein Structure, Function, and Dynamics: a Perspective from Experiments and Theory. *J. Membr. Biol.* **248**, 611–640 (2015).
3. Shaw, D. E. *et al.* Atomic-level characterization of the structural dynamics of proteins. *Science (80-.).* **330**, 341–346 (2010).
4. Boehr, D. D., Nussinov, R. & Wright, P. E. The role of dynamic conformational ensembles in biomolecular recognition. *Nature Chemical Biology* vol. 5 789–796 (2009).
5. Drew, D. & Boudker, O. Shared Molecular Mechanisms of Membrane Transporters. *Annu. Rev. Biochem.* **85**, 543–572 (2016).
6. Kazmier, K., Claxton, D. P. & Mchaourab, H. S. Alternating access mechanisms of LeuT-fold transporters: trailblazing towards the promised energy landscapes. *Curr. Opin. Struct. Biol.* **45**, 100–108 (2017).
7. Wang, J., Hua, T. & Liu, Z. J. Structural features of activated GPCR signaling complexes. *Curr. Opin. Struct. Biol.* **63**, 82–89 (2020).
8. Gusach, A. *et al.* Beyond structure: emerging approaches to study GPCR dynamics. *Curr. Opin. Struct. Biol.* **63**, 18–25 (2020).
9. Ovchinnikov, S. *et al.* Large-scale determination of previously unsolved protein structures using evolutionary information. *Elife* **4**, 1–25 (2015).
10. Nicoludis, J. M. & Gaudet, R. Applications of sequence coevolution in membrane protein biochemistry. *Biochim. Biophys. Acta - Biomembr.* **1860**, 895–908 (2018).
11. Jumper, J. *et al.* Highly accurate protein structure prediction with AlphaFold. *Nature* (2021) doi:10.1038/s41586-021-03819-2.
12. Tunyasuvunakool, K. *et al.* Highly accurate protein structure prediction for the human proteome. *Nature* (2021) doi:10.1038/s41586-021-03828-1.
13. Pereira, J. *et al.* High-accuracy protein structure prediction in CASP14. *Proteins Struct. Funct. Bioinforma.* 1–13 (2021) doi:10.1002/prot.26171.
14. Jumper, J. *et al.* Applying and improving AlphaFold at CASP14 . *Proteins Struct. Funct. Bioinforma.* (2021) doi:10.1002/prot.26257.
15. del Alamo, D., Govaerts, C. & Mchaourab, H. S. AlphaFold2 predicts the inward-facing conformation of the multidrug transporter LmrP. *Proteins Struct. Funct. Bioinforma.* 10–12 (2021) doi:10.1002/prot.26138.
16. Debruycker, V. *et al.* An embedded lipid in the multidrug transporter LmrP suggests a mechanism for polyspecificity. *Nat. Struct. Mol. Biol.* **27**, 829–835 (2020).
17. Martens, C. *et al.* Lipids modulate the conformational dynamics of a secondary multidrug transporter. *Nat. Struct. Mol. Biol.* **23**, 744–751 (2016).
18. Masureel, M. *et al.* Protonation drives the conformational switch in the multidrug transporter LmrP. *Nat. Chem. Biol.* **10**, 149–155 (2014).
19. Yan, R., Zhao, X., Lei, J. & Zhou, Q. Structure of the human LAT1–4F2hc heteromeric amino acid transporter complex. *Nature* **568**, 127–130 (2019).
20. Yan, R. *et al.* Mechanism of substrate transport and inhibition of the human LAT1-4F2hc amino acid transporter. *Cell Discov.* **7**, (2021).
21. Xue, J., Xie, T., Zeng, W., Jiang, Y. & Bai, X. C. Cryo-EM structures of human ZnT8 in both outward-and inward-facing conformations. *Elife* **9**, 1–32 (2020).

22. Wang, N. *et al.* Structural basis of human monocarboxylate transporter 1 inhibition by anti-cancer drug candidates. *Cell* **184**, 370-383.e13 (2021).
23. Bavnhøj, L., Paulsen, P. A., Flores-Canales, J. C., Schiøtt, B. & Pedersen, B. P. Molecular mechanism of sugar transport in plants unveiled by structures of glucose/H+ symporter STP10. *Nat. Plants* **7**, 1409–1419 (2021).
24. Garibsingh, R. A. A. *et al.* Rational design of ASCT2 inhibitors using an integrated experimental-computational approach. *Proc. Natl. Acad. Sci. U. S. A.* **118**, (2021).
25. Garaeva, A. A., Guskov, A., Slotboom, D. J. & Paulino, C. A one-gate elevator mechanism for the human neutral amino acid transporter ASCT2. *Nat. Commun.* **10**, 1–8 (2019).
26. Liang, Y.-L. *et al.* Structure and Dynamics of Adrenomedullin Receptors AM1 and AM2 Reveal Key Mechanisms in the Control of Receptor Phenotype by Receptor Activity-Modifying Proteins. *ACS Pharmacol. Transl. Sci.* **3**, 263–284 (2020).
27. Josephs, T. M. *et al.* Structure and dynamics of the CGRP receptor in apo and peptide-bound forms. *Science (80-.).* **372**, eabf7258 (2021).
28. Ehrenmann, J. *et al.* High-resolution crystal structure of parathyroid hormone 1 receptor in complex with a peptide agonist. *Nat. Struct. Mol. Biol.* **25**, 1086–1092 (2018).
29. Zhao, L.-H. *et al.* Structure and dynamics of the active human parathyroid hormone receptor-1. *Science (80-.).* **364**, 148–153 (2019).
30. Xu, L. *et al.* Cryo-EM structure of constitutively active human Frizzled 7 in complex with heterotrimeric Gs. *Cell Res.* (2021) doi:10.1038/s41422-021-00525-6.
31. Yang, S. *et al.* Crystal structure of the Frizzled 4 receptor in a ligand-free state. *Nature* **560**, 666–670 (2018).
32. Zhang, Y. & Skolnick, J. Scoring function for automated assessment of protein structure template quality. *Proteins Struct. Funct. Genet.* **57**, 702–710 (2004).
33. Zhang, Y. & Skolnick, J. TM-align: A protein structure alignment algorithm based on the TM-score. *Nucleic Acids Res.* **33**, 2302–2309 (2005).
34. Xu, J. & Zhang, Y. How significant is a protein structure similarity with TM-score = 0.5? *Bioinformatics* **26**, 889–895 (2010).
35. Saldaño, T. *et al.* Impact of protein conformational diversity on AlphaFold predictions. *bioRxiv* 1–20 (2021).
36. Mariani, V., Biasini, M., Barbato, A. & Schwede, T. IDDT: A local superposition-free score for comparing protein structures and models using distance difference tests. *Bioinformatics* **29**, 2722–2728 (2013).
37. Zheng, Y. *et al.* Structure of CC Chemokine Receptor 5 with a Potent Chemokine Antagonist Reveals Mechanisms of Chemokine Recognition and Molecular Mimicry by HIV. *Immunity* **46**, 1005-1017.e5 (2017).
38. Zhang, H. *et al.* Structural basis for chemokine recognition and receptor activation of chemokine receptor CCR5. *Nat. Commun.* **12**, 1–12 (2021).
39. Coleman, J. A., Green, E. M. & Gouaux, E. X-ray structures and mechanism of the human serotonin transporter. *Nature* **532**, 334–339 (2016).
40. Coleman, J. A. *et al.* Serotonin transporter–ibogaine complexes illuminate mechanisms of inhibition and transport. *Nature* **569**, 141–145 (2019).
41. Tanaka, Y. *et al.* Structural basis for the drug extrusion mechanism by a MATE multidrug transporter. *Nature* **496**, 247–251 (2013).
42. Zakrzewska, S. *et al.* Inward-facing conformation of a multidrug resistance MATE family transporter. *Proc. Natl. Acad. Sci. U. S. A.* **116**, 12275–12284 (2019).
43. Kuk, A. C. Y., Mashalidis, E. H. & Lee, S.-Y. Crystal structure of the MOP flippase MurJ in

an inward-facing conformation. *Nat. Struct. Mol. Biol.* **24**, 171–176 (2017).
44. Kuk, A. C. Y., Hao, A., Guan, Z. & Lee, S. Y. Visualizing conformation transitions of the Lipid II flippase MurJ. *Nat. Commun.* **10**, (2019).
45. Claxton, D. P., Jagessar, K. L. & Mchaourab, H. S. Principles of Alternating Access in Multidrug and Toxin Extrusion (MATE) Transporters. *J. Mol. Biol.* **433**, 166959 (2021).
46. Crawley, S. W. *et al.* Autophosphorylation activates Dictyostelium myosin II heavy chain kinase A by providing a ligand for an allosteric binding site in the α-kinase domain. *J. Biol. Chem.* **286**, 2607–2616 (2011).
47. Ollikainen, N., Smith, C. A., Fraser, J. S. & Kortemme, T. *Flexible backbone sampling methods to model and design protein alternative conformations*. *Methods in Enzymology* vol. 523 (Elsevier Inc., 2013).
48. Ping, Y. Q. *et al. Structures of the glucocorticoid-bound adhesion receptor GPR97–Go complex*. *Nature* vol. 589 (Springer US, 2021).
49. Pak, M. A. *et al.* Using AlphaFold to predict the impact of single mutations on protein stability and function. *bioRxiv* 2021.09.19.460937 (2021).
50. Akdel, M. *et al.* A structural biology community assessment of AlphaFold 2 applications. *bioRxiv* 2021.09.26.461876 (2021).
51. Martens, C. *et al.* Direct protein-lipid interactions shape the conformational landscape of secondary transporters. *Nat. Commun.* **9**, 1–12 (2018).
52. Muller, M. P. *et al.* Characterization of Lipid–Protein Interactions and Lipid-Mediated Modulation of Membrane Protein Function through Molecular Simulation. *Chem. Rev.* **119**, 6086–6161 (2019).
53. Immadisetty, K., Hettige, J. & Moradi, M. Lipid-Dependent Alternating Access Mechanism of a Bacterial Multidrug ABC Exporter. *ACS Cent. Sci.* **5**, 43–56 (2019).
54. Mirdita, M., Ovchinnikov, S. & Steinegger, M. ColabFold - Making protein folding accessible to all. *bioRxiv* 2021.08.15.456425 (2021).
55. Steinegger, M. & Söding, J. MMseqs2 enables sensitive protein sequence searching for the analysis of massive data sets. *Nat. Biotechnol.* **35**, 1026–1028 (2017).
56. Needleman, S. B. & Wunsch, C. D. A general method applicable to the search for similarities in the amino acid sequence of two proteins. *J. Mol. Biol.* **48**, 443–453 (1970).
57. Madeira, F. *et al.* The EMBL-EBI search and sequence analysis tools APIs in 2019. *Nucleic Acids Res.* **47**, W636–W641 (2019).
58. Roe, D. R. & Cheatham, T. E. PTRAJ and CPPTRAJ: Software for processing and analysis of molecular dynamics trajectory data. *J. Chem. Theory Comput.* **9**, 3084–3095 (2013).

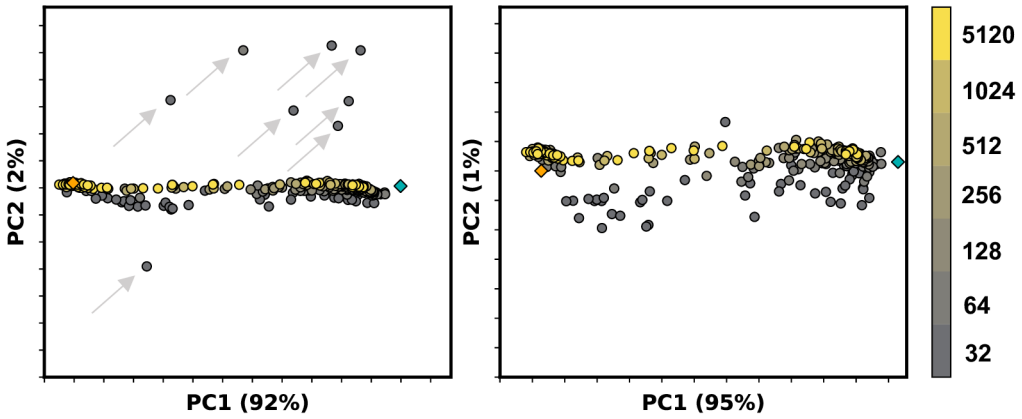

Figure 1 - figure supplement 1. Example PCA of ASCT2 models generated by AF2 containing outlier models. Colors correspond to MSA depth in sequences, while orange and teal diamonds refer to the outward-facing and inward-facing experimental structures, respectively. Left: Outlier models are indicated by grey arrows and could be clearly delineated along PC2. Right: Removal of these models reveal collective variables along PC2.

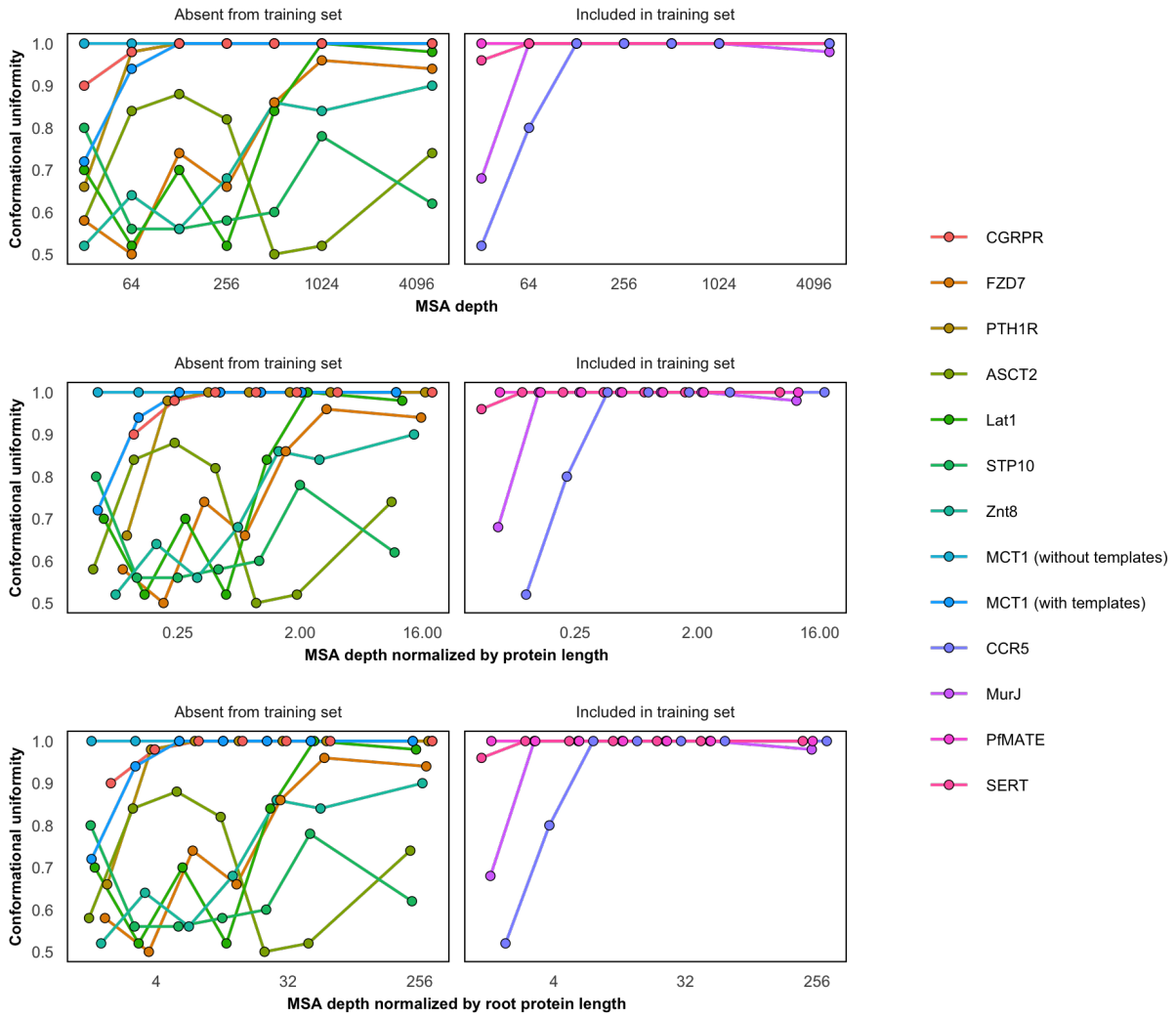

Figure 1 - figure supplement 2. Conformational homogeneity as a function of MSA depth. Conformational homogeneity was defined by classifying models as more similar to one of the two experimental structures based on their TM-scores and calculating the fraction of models in the larger group. MCT1 and proteins in the training set (CCR5, MurJ, PfMATE, and SERT) were biased toward one specific conformation (uniformity = 1) even when using shallow MSAs. X-axis shown on log-2 scale for clarity. Models generated using MSAs with 16 sequences were omitted from this figure.

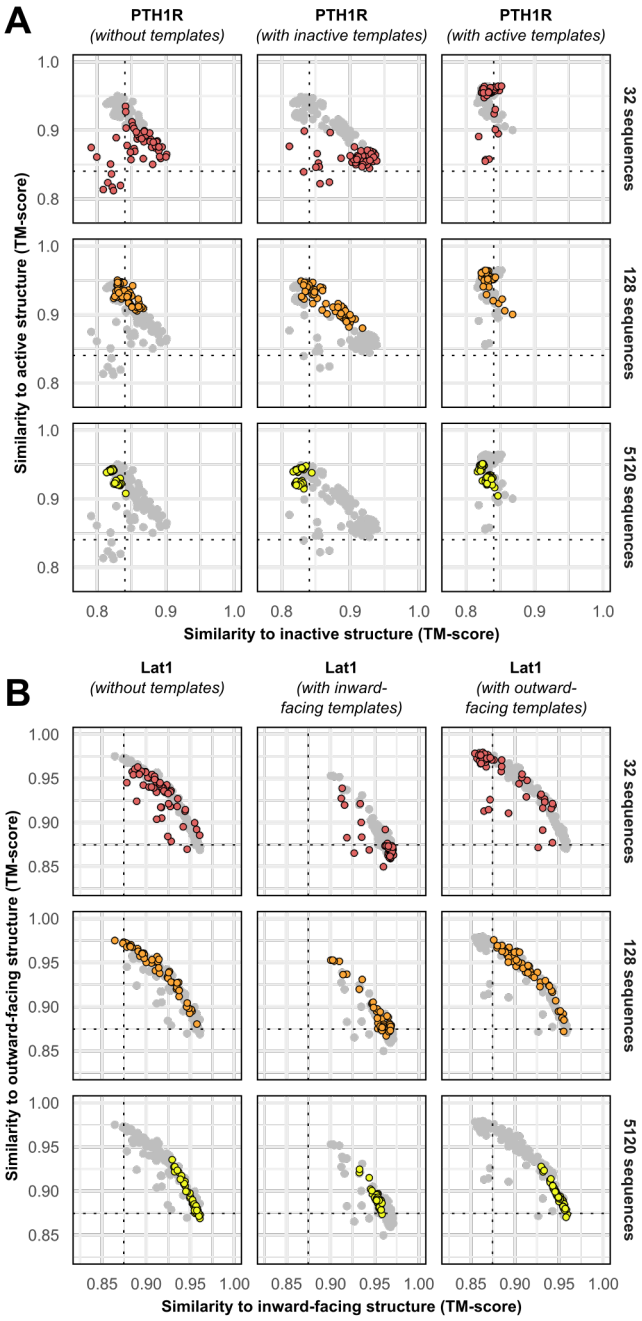

Figure 1 - figure supplement 3. Templates contribute to conformational sampling only when shallow MSAs are provided. (A) PTH1R. **(B)** LAT1.

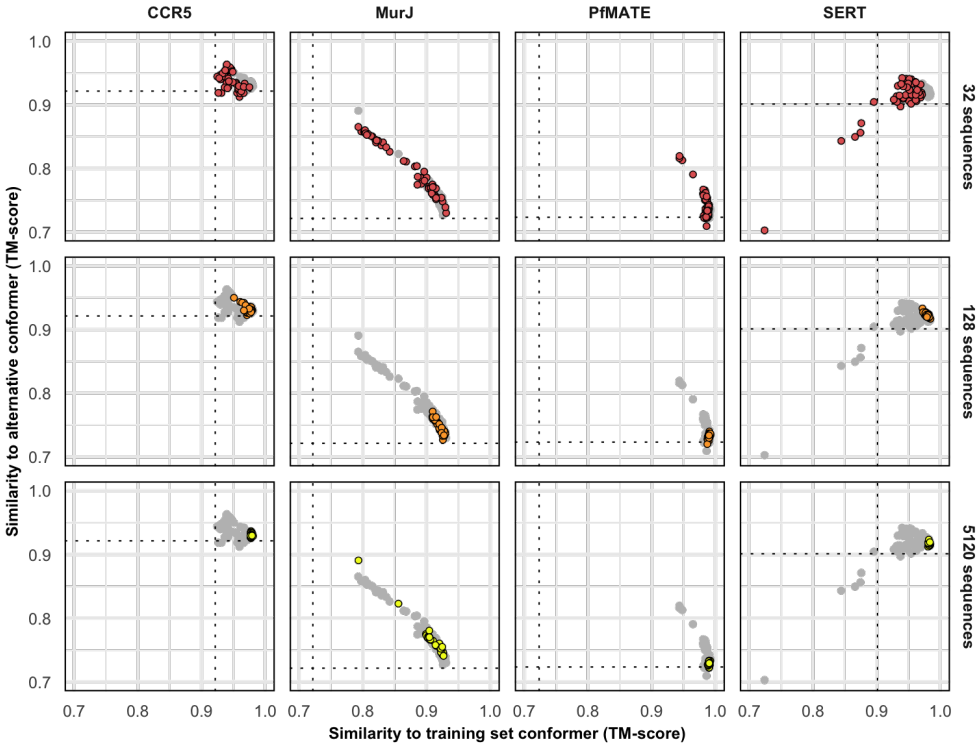

Figure 1 - figure supplement 4. Protein targets with one conformation in the training set cannot be predicted in the alternative conformation. The following experimental structures served as references for the training and the alternative conformations, respectively: 5UIWr and 7F1Qr (CCR5), 5T77a and 6NC9a (MurJ), 3VVNa and 6FHZa (PfMATE), and 5I6Xa and 6DZZa (SERT).

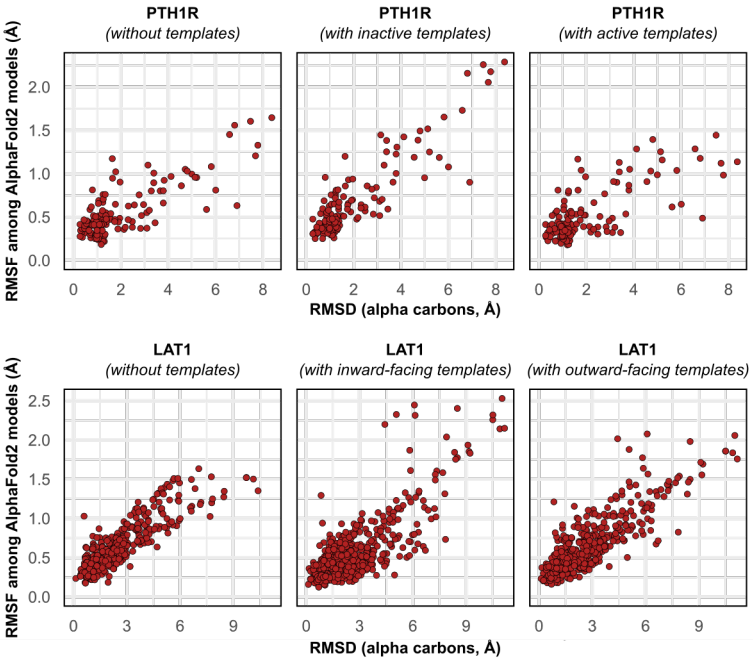

Figure 2 - figure supplement 1. Comparison between each residue's C_α RMSD in the two experimental structures of PTH1R and LAT1 and their RMSF values among AF2 models generated with templates.

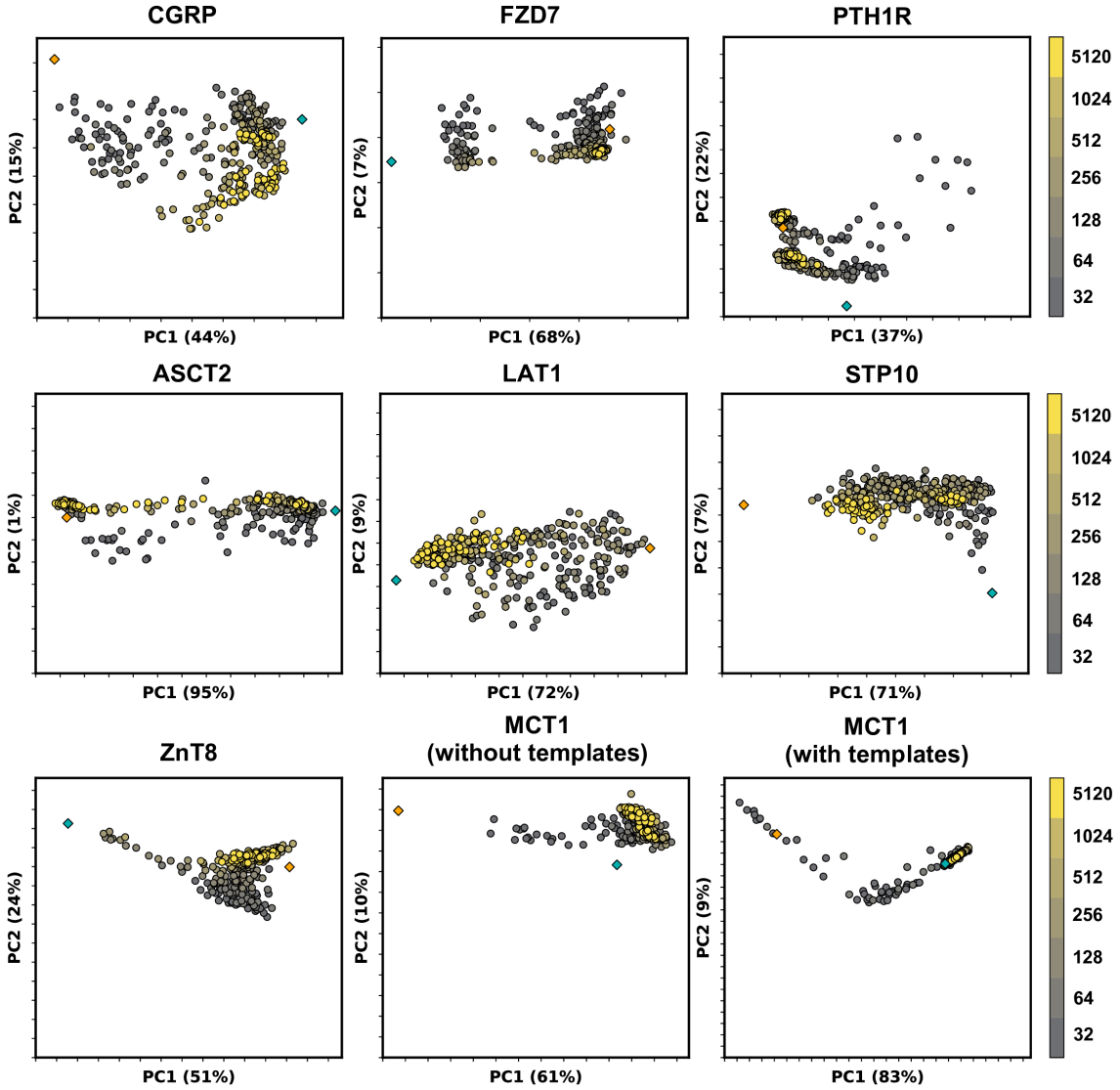

Figure 3 - figure supplement 1. Models sampled by AF2 in multiple conformations cannot be fully explained by linear interpolation of two end structures. Principal component analysis (PCA) of AF2 models, with colors corresponding to the depth of the MSAs used for prediction. Experimental structures in an inward-facing or inactive state are shown as teal diamonds, while structures in an outward-facing or active state are shown as orange diamonds.

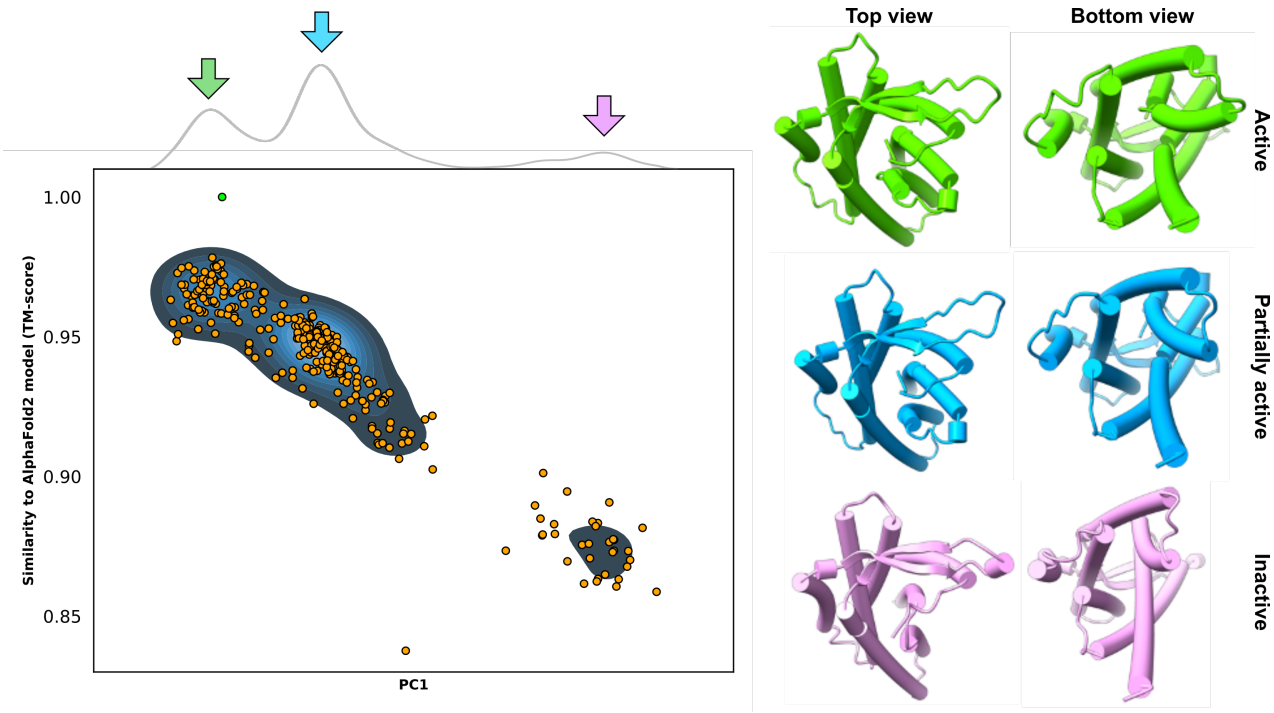

Figure 3 - figure supplement 2. Example predictions of the adhesion GPCR GPR114/AGRG5. Top: Kernel density estimate of the first principal component (PC1) following PCA on all AF2 models. **Bottom:** Comparison of PC1 and TM-score values; alignments were measured from the AF2 database model, which is indicated by the green dot. **Right:** Models extracted from the cluster centers appear to adopt three distinct conformations.